

Make Dark Matter Charged Again

**Prateek Agrawal, Francis-Yan Cyr-Racine, Lisa Randall and
Jakub Scholtz**

Department of Physics, Harvard University,
Cambridge, MA 02138, U.S.A.

E-mail: prateekagrwal@fas.harvard.edu, fcyrraci@physics.harvard.edu,
randall@physics.harvard.edu, jscholtz@physics.harvard.edu

Abstract. We revisit constraints on dark matter that is charged under a $U(1)$ gauge group in the dark sector, decoupled from Standard Model forces. We find that the strongest constraints in the literature are subject to a number of mitigating factors. For instance, the naive dark matter thermalization timescale in halos is corrected by saturation effects that slow down isotropization for modest ellipticities. The weakened bounds uncover interesting parameter space, making models with weak-scale charged dark matter viable, even with electromagnetic strength interaction. This also leads to the intriguing possibility that dark matter self-interactions within small dwarf galaxies are extremely large, a relatively unexplored regime in current simulations. Such strong interactions suppress heat transfer over scales larger than the dark matter mean free path, inducing a dynamical cutoff length scale above which the system appears to have only feeble interactions. These effects must be taken into account to assess the viability of darkly-charged dark matter. Future analyses and measurements should probe a promising region of parameter space for this model.

Keywords: dark matter theory, dwarfs galaxies, galaxy evolution, rotation curves of galaxies

ArXiv ePrint: [1610.04611](https://arxiv.org/abs/1610.04611)

Contents

1	Introduction	1
2	Model	2
2.1	Relic abundance	3
3	Constraints and Phenomenology	3
3.1	Ellipticity	3
3.1.1	Review of the timescale calculation	6
3.1.2	Evolution of the velocity anisotropy	7
3.1.3	Ellipticity and Density as a function of radius	9
3.2	Dwarf Galaxy Survival	10
3.3	Merging Cluster Constraints	12
4	For the Future	13
4.1	Cores in Very Strongly Interacting Systems	14
5	Conclusions	16
A	Scattering Cross-section	17
B	Differential equation for velocity anisotropy	18

1 Introduction

Apart from its manifold gravitational influences, dark matter has so far eluded detection, prompting model builders to think more broadly about what dark matter can be and in the process consider other and more subtle ways to search for it. One intriguing possibility has always been charged dark matter, with dark matter charged under its own force that Standard Model particles do not necessarily experience. This can constitute all of the dark matter, as has been considered in Refs. [1–33], or it can be a fraction of the dark matter, as was studied in Refs. [34–37]. More generally, research on self-interacting dark matter has been motivated in part by potential discrepancies in conventional dark matter scenarios, especially on small scales. However, most papers on charged dark matter imply that it is very restricted by current constraints.

It is of interest to ask whether dark matter is necessarily constrained to have only very tiny or short-ranged interactions. An immediate concern is that new interactions in the dark sector – especially those involving massless particles – could significantly delay the epoch of dark matter kinetic decoupling and affect the large-scale structure of the Universe. However, for dark matter with a weak-scale mass, such bounds are generally much weaker [7, 8, 38, 39] than those coming from collapsed dark matter structures such as clusters, galaxies and dwarves. This paper thus focuses on these latter objects.

Charged dark matter – even when charged under an invisible new $U(1)$ – can potentially lead to observable differences in the dark matter density distribution that can be helpful when searching for interactions (see e.g. [40–48]), but can also in principle impose serious

constraints. This model, which we shall refer to here as darkly-charged dark matter, is simple from a particle physics perspective but leads to extremely interesting consequences in astrophysics. Constraints arise from the triaxiality of galaxy and cluster-scale dark matter halos, since overly strong interactions can wipe out deviations from isotropy. A somewhat weaker constraint can be derived from observations of merging galaxy clusters [49–59]. A further constraint comes from the survival of dwarf galaxies as they move through the halo [54, 55, 60].

In this paper we revisit the constraints on dark matter charged under its own $U(1)$ to show that the allowed parameter space is broader than implied by the literature. We show explicitly that even with pre-existing assumptions, the literature overestimates the bound by about an order of magnitude. Furthermore these constraints might be less reliable than assumed due to uncertainties in initial conditions, for example. Our result is important because it opens the window for charged dark matter as light as the weak scale, even if it carries a charge as strong as that of electromagnetism. It is also of interest for Double-Disk dark matter Ref. [61] as it opens the possibility of all dark matter being charged while allowing a dark matter disk. We also suggest interesting implications for charged dark matter that have not yet been investigated, including using the radial dependence of ellipticity to disentangle the impact of velocity anisotropies from that of anisotropic potentials, and the modification of the dwarf galaxy populations in both mass and internal structure, with important consequences for small-scale issues [62–65].

Dark matter self-interactions through the dark photon are strongly enhanced for low velocity systems such as dwarf galaxies. The coupling strengths allowed by our revised constraints lead to extremely large cross sections in dwarf galaxies – a relatively unexplored regime in self-interaction dark matter (SIDM) simulations – while being roughly consistent with the desired SIDM cross sections required to solve potential issues at galaxy and cluster scales [46]. Generally, many SIDM models invoke a massive mediator to cut off strong interactions at low velocities. Interestingly, our very strong interactions can inhibit heat transfer over scales larger than the dark matter mean free path, inducing a dynamical cutoff length scale above which the system appears to have only feeble interactions [66–69]. Such a dynamical cutoff would likely obviate the need of introducing the cutoff through the mass of the mediator.

The outline of this paper is as follows. We introduce the model in section 2. In section 3.1 we study the strongest constraint quoted in the literature, the ellipticity constraint, and point out reasons why the actual bounds might be weaker. This makes the constraints coming from dwarf galaxies the most stringent, which we study in section 3.2. We briefly discuss the constraints from merging galaxy clusters in section 3.3. We highlight future work in section 4, emphasizing the importance of the strongly interacting regime at low velocities in section 4.1, and finally conclude in section 5.

2 Model

We consider a simple model with a Dirac fermion X of weak-scale mass m_X , charged under a new dark $U(1)$ gauge symmetry with gauge boson γ_D . The Lagrangian is

$$\mathcal{L} = -\frac{1}{4}V_{\mu\nu}V^{\mu\nu} + \bar{X}i\not{D}X - m_X\bar{X}X, \quad (2.1)$$

where V_μ is the dark photon and $D_\mu = \partial_\mu + ig_D V_\mu$. We also define $4\pi\alpha_D = g_D^2$. We assume that there is no kinetic mixing between photons and the dark photons. In order to

avoid conflict with cosmic microwave background (CMB) measurements of the abundance of relativistic species [70], we take the dark photon bath temperature T_D to be half that of the CMB photon, $\xi \equiv T_D/T_{\text{SM}} = 0.5$. In this simple model, the dark matter relic abundance can be set by a thermal freezeout, which we briefly review in the next section.

2.1 Relic abundance

The relic abundance is determined by the freezeout process $X\bar{X} \rightarrow \gamma_D\gamma_D$ with a leading thermally averaged cross-section given by

$$\langle\sigma v_{\text{Møll}}\rangle = \frac{\pi\alpha_D^2}{m_X^2}\bar{S}_{\text{ann}}(\alpha), \quad (2.2)$$

where we follow Ref. [71] definition of Møller velocity. The Sommerfeld enhancement \bar{S}_{ann} is important for $\pi\alpha_D/v_f \gtrsim 1$, which arises for large $m_X \gtrsim 1$ TeV. We use the results of Ref. [72] to include the thermally averaged Sommerfeld enhancement.

Ref. [71] gives the corresponding relic density for this cross-section:

$$\Omega_X = \frac{16\pi^3}{9\sqrt{5}\pi} \frac{g_0^*}{\sqrt{g_{\text{eff}}}} \frac{T_0^3}{M_{\text{pl}}^3} \frac{x_f}{\langle\sigma v_{\text{Møll}}\rangle H_0^2}, \quad (2.3)$$

where T_0 is the CMB temperature today, H_0 the Hubble constant today, M_{pl} is the Planck mass, g_0^* is the effective number of relativistic degrees of freedom today, while g_{eff} is the effective number of degrees of freedom at freezeout, which happens when $T_f = m_X/x_f$. We can determine x_f as a solution to the equation

$$\xi^{3/2} \frac{\sqrt{45}}{8\pi^2} \frac{g_X}{\sqrt{g_*(T_f)}} \frac{\alpha_D^2 M_{\text{pl}}}{m_X} \delta(\delta + 2) = \omega = \sqrt{x_f} e^{x_f/\xi}, \quad (2.4)$$

where we denote the number of degrees of freedom in X by g_X and $\delta \sim 1.5$ is a matching parameter to the exact numerical solution (x_f is only logarithmically sensitive to δ). We use the approximate solution [6],

$$x_f = \xi \log \omega - \frac{1}{2} \xi \log(\xi \log \omega), \quad (2.5)$$

and require that $\Omega_X = 0.265$ [70] in order to obtain α_D as a function of m_X . We note that it is both possible to decrease and increase α_D for a given value of m_X . We can decrease α_D by opening another annihilation channel for X , and increase α_D by introducing additional contributions to Ω_{DM} . Assuming no other freezeout channels and that X is the only contribution to Ω_{DM} , we show our result for relic abundance in figure 4.

3 Constraints and Phenomenology

3.1 Ellipticity

One of the strongest purported constraints on charged dark matter comes from observed triaxial structure of galaxy halos. Self-interacting dark matter can in principle reduce the degree of anisotropy by creating a more isotropic dark matter velocity distribution. By measuring non-zero ellipticity of the gravitational potential of NGC720, Ref. [73] have made it possible to obtain constraints on self-interaction strength of dark matter. Ref. [8] have used

this data to put bounds on self-interacting dark matter. These authors considered both hard interactions, where large momentum exchange immediately reduces anisotropy significantly and soft exchanges, where the cumulative effect of many interactions of a dark matter particle as it passes through the galaxy serves to make the velocity distribution more isotropic. The latter is the more important process: even though each collision changes the momentum of a particle by a small amount a single dark matter particle can scatter many times during its orbits over the lifetime of the galaxy.

We review the calculation in the literature, highlighting aspects which modify the bounds. The usual calculation involves obtaining the characteristic timescale for an average particle to change its kinetic energy by an $\mathcal{O}(1)$ factor, and interpreting this as the timescale τ_{iso} on which the velocity vector fully randomizes. We present the detailed calculation below; the final result is [8]

$$\tau_{\text{iso}} = \mathcal{N} \frac{m_X^3 v_0^3}{\alpha_D^2 \rho_X} \left(\log \frac{(b_{\text{max}} m_X v_0^2 / \alpha_D)^2 + 1}{2} \right)^{-1} = \mathcal{N} \frac{m_X^3 v_0^3}{\alpha_D^2 \rho_X} (\log \Lambda)^{-1}. \quad (3.1)$$

We comment on the numerical prefactor \mathcal{N} below. There are two qualitatively important aspects of our analysis:

- In NGC720 the baryonic component dominates the enclosed gravitational mass until about $r \sim 6$ kpc [74]. Therefore, ellipticity measurements within this radius do not constrain the dark matter potential. We choose to apply the ellipticity constraint at $r = 6$ kpc where the isotropization rate is relatively smaller due to a lower dark matter density.
- The long range interactions between dark matter are screened at the inter-particle spacing in the galaxy (or galaxy cluster). Typically the screening length is taken to be the Debye screening length λ_D . However, in a neutral plasma with equal mass opposite charges, if the inter-particle spacing $\lambda_{pp} \ll \lambda_D$, then the contributions to scattering from individual charges cancel* leaving behind terms of order λ_{pp}/λ_D . As a result it is appropriate to take the inter-particle spacing as the screening length

Our numerical prefactor is

$$\mathcal{N} = \frac{3}{16\sqrt{\pi}}. \quad (3.2)$$

While we agree on the functional form of the timescale, this prefactor is somewhat different from Ref. [8]. This difference is accounted for by a different choice of r (3 kpc), IR cutoff (Debye mass) and some other numerical factors (normalization of velocity, cross section and energy transfer) in that work. Consequently, our isotropization timescale is larger by a factor

$$\underbrace{\frac{3}{2}}_{\log \Lambda} \times \underbrace{\frac{3}{1}}_{\rho} \times \underbrace{\frac{1}{4}}_{d\sigma/d\Omega} \times \underbrace{\frac{3}{2}}_{\langle v^2 \rangle = 3v_0^2/2} \times \underbrace{\frac{2}{1}}_{\delta E_k} = \frac{27}{8}. \quad (3.3)$$

Moreover, there are additional considerations whose numerical effects require explicit additional calculations we will present in section 3.1.2 and 3.1.3:

*One can alternatively see this as scattering on dipoles, which do not contribute to the logarithmic (dominant) part of the cross-section integral.

- It is not sufficient to simply calculate the interaction rate, or even the rate at which energy transfers from one velocity component to another. The rate at which the interaction occurs is sensitive to velocity anisotropy. As the initially smaller component of the velocity grows comparable to the larger one, the rate of energy transfer slows down. (Otherwise the smaller one would continue to grow indeterminately which of course is not the case.) This saturation effect can relax the bounds from ellipticity significantly.
- Furthermore, the constraint depends on the radius at which the ellipticity is measured. This is important because the best ellipticity measurements apply in the outer regions of galaxies where the density is lowest and therefore interactions are less frequent.

Finally there are additional challenges to ellipticity measurements as constraints on dark matter self-interactions that shed doubt on the viability of ellipticity measurements as constraints on dark matter self-interaction rate:

- The measured ellipticity of the gravitational potential is due to anisotropy in the density of the dark matter distribution. All authors constraining loss of ellipticity calculate the rate of energy transfer, which might apply to heat flow among different radii or between different velocity components. We can estimate the rate at which the velocity distribution becomes isotropic through a calculation, but the rate at which the density distribution (and the gravitational potential) becomes isotropic requires N-body simulations, as discussed in Ref. [75]. In isolated static haloes one can argue that the approach to isotropy is the same for velocity distribution and density distribution because the same collisional term contributes to the change of the distribution function. However, substructure, dark matter streams, accretion, rotation or long relaxation time can change this expectation. As a result, the ellipticity bound on dark matter self-interaction may be weaker than that obtained from the requirement on isotropy in velocity distribution alone.
- The constraint from galaxies is stronger than the constraint from galaxy clusters. But the former relies on only a single galaxy NGC720, which might not be representative. As this galaxy does not exhibit strong ellipticity, it might be undergoing isotropization at a diminished rate as the velocity components become more comparable. In any case, having access to a larger statistical sample of galaxy ellipticities is key to make this type of constraint robust.
- The history of the galaxy is a key input that observations do not have access to. Recent mergers can contribute to a large ellipticity even in the presence of strong interactions. Even if a deviation from the cold dark matter (CDM) prediction is expected, ellipticity observations are sensitive to the initial distribution, so robust conclusions can only be drawn from observables that distinguish CDM and Darkly Charged dark matter independently of initial conditions.

Given the latter items, even our more careful analysis very likely overstates the constraint as we calculate the rate at which the velocity components equilibrate but even a galaxy with isotropic velocity distribution can exhibit ellipticity in its potential. Nonetheless, because it might be useful for future analyses, and also to show that weak scale dark matter is viable even if isotropy of velocities in galaxies is a serious constraint, we present the more careful computation here.

3.1.1 Review of the timescale calculation

In this section we review the calculation of the timescale for an average dark matter particle to change its kinetic energy E_k by an $\mathcal{O}(1)$ factor. We define this timescale as

$$\tau_{\text{iso}} = \frac{\langle E_k \rangle}{\langle \dot{E}_k \rangle}, \quad (3.4)$$

where the $\langle \cdot \rangle$ denotes thermal averaging. The average rate of change of energy of a typical particle is

$$\langle \dot{E} \rangle = \int d\Omega dv \frac{d\sigma}{d\Omega} f(v) \delta E_k v n_X, \quad (3.5)$$

where n_X is the number density of X particles. For two equal mass particles with velocities v_1 and v_2 , the energy loss/gain after a collision is $\delta E_k = \pm(1 - \cos \theta_{\text{cm}})m(v_1^2 - v_2^2)/4$, where θ_{cm} is the final scattering angle in the center-of-mass (CM) frame. The differential cross section is (see Appendix A)

$$\frac{d\sigma}{d\Omega} = \frac{4\alpha_D^2}{m_X^2 |v_1 - v_2|^4 (1 - \cos \theta_{\text{cm}})^2}. \quad (3.6)$$

We assume a Maxwell-Boltzmann distribution with dispersion v_0 for the dark matter velocities. This yields

$$\langle \dot{E} \rangle = \frac{4\pi\alpha_D^2\rho_X}{2m_X^2} \int_{\theta_{\min}} \frac{1 - \cos \theta_{\text{cm}}}{(1 - \cos \theta_{\text{cm}})^2} d\cos \theta_{\text{cm}} \int \frac{4vdv}{\sqrt{\pi}v_0^3} \exp\left(-\frac{v^2}{v_0^2}\right), \quad (3.7)$$

where $\rho_X = m_X n_X$ is the dark matter energy density. Since the leading contribution from positively and negatively charged particles will cancel, we use the inter-particle spacing ($\lambda_P = (m_X/\rho_X)^{1/3}$) as an infrared cutoff for the impact parameter. The relationship between largest impact parameter $b_{\max} = \lambda_P$ and angle of scattering is

$$\frac{\theta_{\min}}{2} = \cot^{-1} \frac{\lambda_P m_X v_0^2}{\alpha_D}. \quad (3.8)$$

Therefore,

$$\langle \dot{E} \rangle = \frac{4\sqrt{\pi}}{v_0} \frac{\alpha_D^2 \rho_X}{m_X^2} \log \left[1 + \frac{\lambda_P^2 m_X^2 v_0^4}{\alpha_D^2} \right] \equiv \frac{4\sqrt{\pi}}{v_0} \frac{\alpha_D^2 \rho_X}{m_X^2} \log \Lambda. \quad (3.9)$$

The timescale to make the velocity distribution isotropic is then

$$\tau_{\text{iso}} = \frac{3}{16\sqrt{\pi}} \frac{m_X^3 v_0^3}{\alpha_D^2 \rho_X \log \Lambda}. \quad (3.10)$$

As noted above, the prefactor differs from the calculation in [8] by the factor outlined in Eq. (3.3).

This calculation gives the rate at which a large initial ellipticity decreases, but does not suffice to determine the time it takes to erase relatively small ellipticities, for which all velocity components are substantial and comparable. We address this issue in the next section, where we explicitly calculate the time to erase ellipticity for different measured ellipticity values.

3.1.2 Evolution of the velocity anisotropy

In this section, we illustrate how the transfer of energy from a hot population to a colder one evolves as a function of time. This would apply either to energy transferring over different radii or for energy transfer from a velocity distribution in one direction to a velocity component along another axis. Here we model ellipticity (defined by the ratio of lengths of semi-minor axis, b , and semi-major axis, a) as an anisotropy in velocity distribution (a strong assumption). In particular, in a virialized halo, $\langle v^2 \rangle \sim R^{-1}$ and therefore:

$$\epsilon = 1 - \frac{b}{a} \sim 1 - \frac{\langle v_a^2 \rangle}{\langle v_b^2 \rangle}. \quad (3.11)$$

The timescale calculation above estimates the growth of ellipticity only when $\langle v_a^2 \rangle \ll \langle v_b^2 \rangle$, that is for large ellipticities $\epsilon \lesssim 1$. However, when $\langle v_a^2 \rangle \lesssim \langle v_b^2 \rangle$, we expect a much smaller growth of the subleading velocity component because the process is proportional to the velocity anisotropy:

$$\frac{d\langle v_a^2 \rangle}{dt} \propto (\langle v_b^2 \rangle - \langle v_a^2 \rangle)^\gamma, \quad (3.12)$$

where the index γ depends on the type of scattering that is erasing anisotropy. Here, we use a slightly simpler physical system for the sake of clarity to explore this slowing of the decline of ellipticity quantitatively. We study a cold isotropic population of gas with a Maxwellian velocity distribution, with a velocity dispersion v_c . This gas is placed in a hotter bath, with the corresponding dispersion $v_h \gg v_c$. We study the growth of the velocity dispersion of the colder population.

The Boltzmann equation reads

$$\frac{df(v_1)}{dt} = \int d^3v_2 d\Omega' |v_1 - v_2| \frac{d\sigma}{d\Omega'} (f(v_1)f(v_2) - f(v_3)f(v_4)). \quad (3.13)$$

In the above equation the final velocities v_3 and v_4 are uniquely determined by v_1 , v_2 and the scattering angle Ω' . The unprimed quantities are in the galaxy frame, primed quantities are in the CM frame. The definition of the probability distribution function $f(v)$ is

$$f(v) = \frac{n_c}{\pi^{3/2}v_c^3} \exp\left(-\frac{v^2}{v_c^2}\right) + \frac{n_h}{\pi^{3/2}v_h^3} \exp\left(-\frac{v^2}{v_h^2}\right). \quad (3.14)$$

Since the distribution is uniquely determined by v_c , it is sufficient to look at the evolution of the $v_1 = 0$ bin. Since we are setting $v_1 = 0$, the kinematics simplifies and the final velocities in the galaxy frame are

$$v_{3,4}^2 = \frac{1}{2}v_2^2(1 \pm \cos\theta'). \quad (3.15)$$

Finally, the differential cross-section is again

$$\frac{d\sigma}{d\Omega} = \frac{4\alpha_D^2}{m_X^2 |v_1 - v_2|^4 (1 - \cos\theta')^2}. \quad (3.16)$$

With all the pieces ready, we can focus on the evolution of the $v_1 = 0$ bin. The Boltzmann eq. (3.13) tells us (using $\cos\theta' = x$):

$$-\frac{3\dot{v}_c n_c}{\pi^{3/2}v_c^4} - \frac{3\dot{v}_h n_h}{\pi^{3/2}v_h^4} = \frac{4\alpha_D^2}{m_X^2} \int \frac{d^3v_2}{v_2^3} \frac{d\phi' dx}{(1-x)^2} \left(f(0)f(v_2) - f(v_2\sqrt{(1-x)/2})f(v_2\sqrt{(1+x)/2}) \right). \quad (3.17)$$

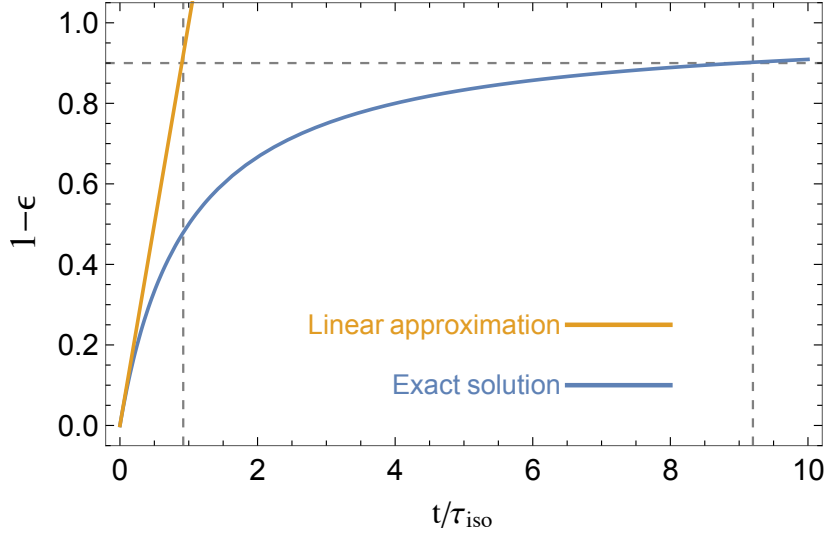


Figure 1: Time evolution of the ellipticity as modeled by our simplified system in section 3.1.2 starting from an ellipticity of order unity. The solid orange line shows the approximate linear evolution, similar to the expansion performed in eq. (3.24). The solid blue curve illustrates the exact solution given in eq. (3.23). The dashed vertical lines illustrate the time to reach an ellipticity of 0.1 in both cases. The saturation effect of the rate of isotropization as the halo becomes more isotropic is clearly visible in the exact solution.

We will neglect the backreaction on the bath, \dot{v}_h . Using rotation invariance, we can perform the angular v_2 integral and the ϕ' integral. Hence,

$$-\frac{3\dot{v}_c}{v_c^4} = \frac{32\pi^3\sqrt{\pi}\alpha_D^2}{m_X^2 n_c} \int \frac{dv_2}{v_2} \frac{dx}{(1-x)^2} \left(f(0)f(v_2) - f(v_2\sqrt{(1-x)/2})f(v_2\sqrt{(1+x)/2}) \right). \quad (3.18)$$

Rather than do the exact integral, we focus instead on the $\theta \rightarrow 0$ ($x \rightarrow 1$) limit, which dominates the behavior. After some algebra (see appendix B) the Boltzmann equation reads

$$\dot{v}_c = -\frac{8\sqrt{\pi}\alpha_D^2 n_h}{3m_X^2 v_h^5 v_c} (v_c^2 - v_h^2)^2 \int_0^{\cos^{-1}\theta_{\min}} \frac{dx}{(1-x)}. \quad (3.19)$$

As before, we use the inter-particle spacing to cut off the infrared divergence above. The result is a first order differential equation for v_c

$$v_c \dot{v}_c = -\frac{8\sqrt{\pi}\alpha_D^2 n_h}{3m_X^2 v_h^5} (v_c^2 - v_h^2)^2 \log \Lambda, \quad (3.20)$$

where Λ is the same as in eq. (3.9), with v_0 replaced by v_h . The solution takes the form

$$v_c^2(t) = v_h^2 - \frac{v_h^2}{\frac{t}{\tau} + \frac{v_h^2}{v_h^2 - v_{c,0}^2}}, \quad (3.21)$$

where $v_{c,0}$ is the initial velocity dispersion of the cold population, and where we have defined an effective timescale to isotropize the velocity distribution:

$$\tau = \frac{3m_X^2 v_h^3}{16\sqrt{\pi}\alpha_D^2 n_h \log \Lambda}. \quad (3.22)$$

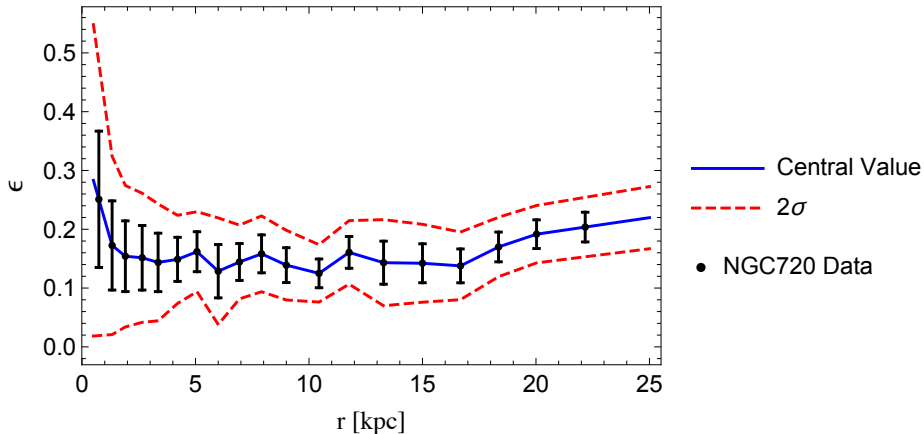


Figure 2: Ellipticity of the NGC720 potential as measured by Ref. [73]. The black data points show the measurements with 1σ error bars. The blue curve is our interpolation of their central values, while the 2σ error bands are in dashed red.

The ellipticity evolves over time as

$$\epsilon(t) \sim 1 - \frac{v_c^2}{v_h^2} = \frac{\epsilon_0}{\frac{t}{\tau}\epsilon_0 + 1}. \quad (3.23)$$

We can see that for small initial dispersion $v_{c,0} \ll v_h$ and $t \ll \tau$,

$$v_c^2 \sim v_h^2 \frac{t}{\tau} = \frac{16\sqrt{\pi}\alpha_D^2 n_h \log \Lambda}{3m_X^2 v_h} \times t. \quad (3.24)$$

However, this early time expansion neglects the saturation effect as the temperature of the cooler component gets comparable to the hotter one. In figure 1 we show that the time taken to get to a small ellipticity can be much longer than the timescale in eq. 3.22. In order to include this effect we need to determine the degree to which the velocity components become isotropic inside the galaxy. Since ellipticity in NGC720 varies with the galactic radius we need to extend our analysis to include radius dependence, which we now turn to in the next section.

3.1.3 Ellipticity and Density as a function of radius

Measuring ellipticity as a function of radius is a complex process. To tackle this challenge, authors of Ref. [73] have adopted an iterative process based on measuring second moments inside elliptical annuli. We show their measurements for NGC720 in figure 2. From eq. (3.10) we see that regions with the highest phase space density ρ/v_0^3 yield the shortest time scales. We use the data of Ref. [74] to determine both the dark matter density and local virial velocity as a function of radius. The shortest times and therefore the strongest constraint would come from the densest regions – the inner most parts of the galaxy. However, the uncertainty on ellipticity is significant for these smaller radii, weakening the overall bound.

For example, the 2σ uncertainty region includes $\epsilon \sim 0$ for the inner most data point and therefore leads to virtually no constraint at all for that radius. We study this effect in figure 3, where we plot as a function of r the time required to reach the ellipticity corresponding to

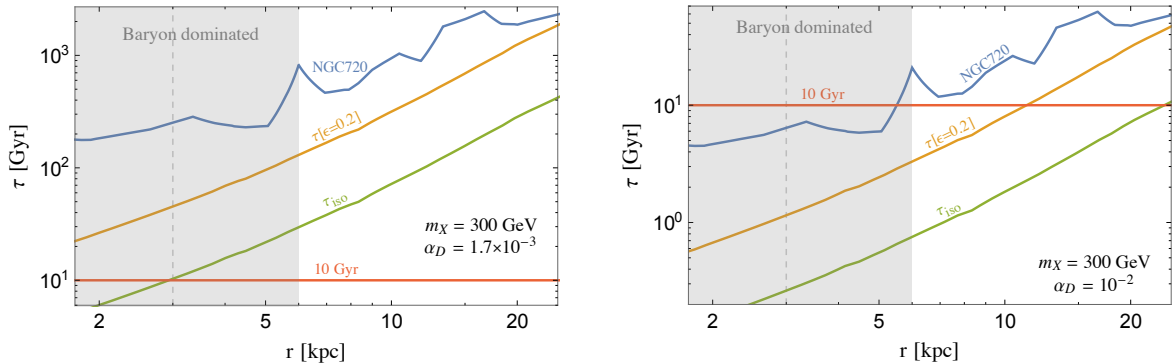


Figure 3: Time to erase galactic ellipticity (caused by velocity anisotropy) through collisions of darkly-charged dark matter particles. The blue curve gives the time to reduce ellipticity in NGC720 down to $\epsilon(r)$ as given by the *lower bound* from figure 2. The orange curve shows the time it takes to reduce ellipticity down to a *fixed, average* $\epsilon = 0.2$ for each r . The green curve shows the timescale τ_{iso} given by eq. (3.1) (adopted from Ref. [8]) where both ρ and v_0 are evaluated as functions of radius as given in Ref. [74]. We show the 10 billion year mark in red and the 3 kpc radius by a dashed vertical line. The grey regions indicate radii for which baryons dominate the gravitational potential of NGC720 and are thus not reliable for constraining ellipticity of the dark matter component. Both panels use $m_X = 300$ GeV but differ in their value of α_D , with the left panel using $\alpha_D = 1.7 \times 10^{-3}$ (which would satisfy Ref. [8]) and the right panel showing $\alpha_D = 10^{-2}$ (which represents the bound from our calculation).

the 2σ lower bound shown in figure 2. We show our results for two values of α_D with a sample mass $m_X = 300$ GeV.

Even when we include the effects of weakening bounds from ellipticity at smaller radii we still obtain strong bounds from the inner regions of the galaxy. However, these inner regions are dominated by the mass of the baryonic component and so the ellipticity of the local gravitational potential is dominated by the baryons. Furthermore, as found by Ref. [76], a thermalized self-interacting dark matter density profile is influenced by the baryonic component. They find that the density ellipticity and the velocity anisotropy for dark matter might not be correlated in the regions where baryons dominate the local potential. As a result, we do not trust the ellipticity measurement as a constraint on dark matter self-interaction for these inner radii. Ref. [77] have constrained the mass components of NGC720 as functions of radius. In their study the dark matter component becomes dominant in mass only after $r \sim 6$ kpc. As a result we will cutoff the constraints on $\alpha_D - m_X$ from the ellipticity measurement at this radius $r = 6$ kpc. Figure 4 shows the resulting ellipticity constraint in the $\alpha_D - m_X$ plane together with other constraints we discuss in the following sections. We note that even this revised constraint is subject to uncertainties, as mentioned in section 3.1.

3.2 Dwarf Galaxy Survival

We now turn to other potential constraints. The strongest such constraint is from dwarf galaxy survival as they orbit in the halo of the host galaxy. With too strong an interaction, dwarf galaxies will be stripped as they pass through a halo. Ref. [54] derived a reasonably strong constraint on dark matter—not quite as strong as the purported ellipticity constraint

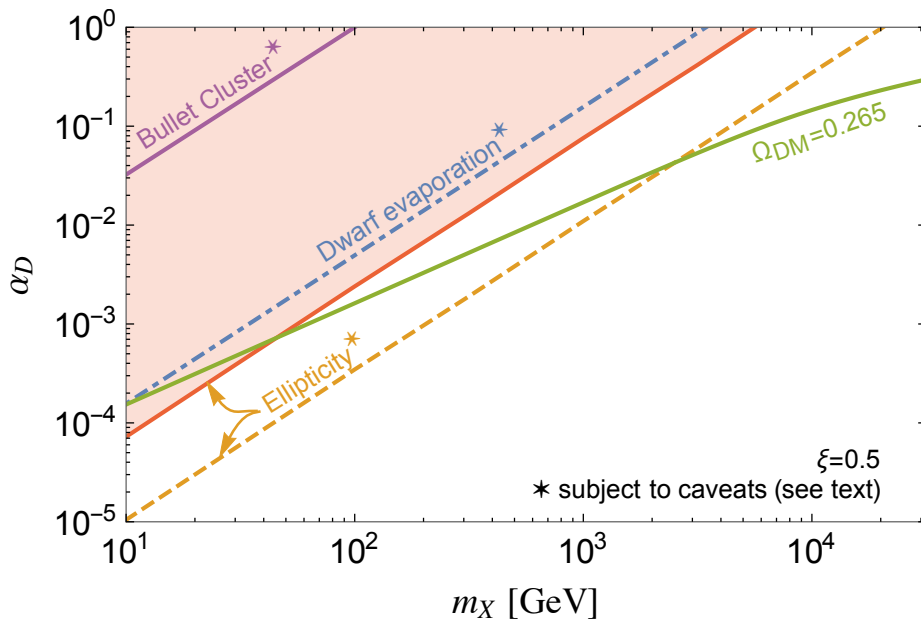


Figure 4: Constraints on the darkly-charged dark matter parameter space in the $m_X - \alpha_D$ plane. Note that the constraints aside from relic abundance have the caveats discussed in the text and should not be taken as strict bounds on the parameter space. The ellipticity constraints (discussed in section 3.1) are presented as two curves: the original Ref. [8] calculation [dashed yellow], and the more complete (though still uncertain) calculation that includes the radius dependent constraints on ellipticity from figure 3 [red]. We also show the constraint from evaporation of Milky Way dwarf galaxies from Ref. [54] and discussed in section 3.2 [dot-dashed blue]. We also display the Bullet cluster bound adopted from Ref. [50] and discussed in section 3.3 [purple]. Finally, we show the $m_X - \alpha_D$ curve for which the freeze-out mechanism discussed in section 2.1 produces the correct relic density for darkly-charged dark matter [green], which includes the effects of Sommerfeld enhancement.

but stronger than that from the Bullet Cluster, for example. Again, they found that numerous soft scatterings dominated over a single hard scattering. As presented in Ref. [54], the constraint reads

$$\frac{\alpha_D^2}{m_X^3} < 10^{-11} \text{ GeV}^{-3}. \quad (3.25)$$

We believe this constraint is also somewhat overstated, both for technical reasons that reduce the bound slightly and for other reasons that could be very interesting, but require a more careful analysis that we delay to a future publication. We do not present the full calculation but rely on the calculation for ellipticity as presented above. The technical disagreements are as follows:

- The same consideration about the cutoff in the infrared logarithm applies here. Putting in the inter-particle spacing rather than the Debye wavelength weakens the numerical value of the bound in eq. (3.25) by about a factor of 2/3.

- Ref. [54] integrates $\cos \theta_{\text{cm}}$ on the interval $[0, 1)$ and then multiply by a factor of 2. This overestimates the cross-section by a factor of 2.
- The analysis assumed a dark matter density of $10^{-26} \frac{\text{g}}{\text{cm}^3}$. Though approximately correct, this is probably a slight overestimate of the density in the region for the relevant dwarf galaxies. Putting in the Carina dwarf galaxy we found the density overestimated by a factor of 3, assuming the dwarf does not spend much time at smaller radius, which was assumed for a conservative bound.

Putting all these factors together:

$$f = \underbrace{\frac{3}{2}}_{\log \Lambda} \times \underbrace{2}_{d\sigma/d\Omega} \times \underbrace{3}_{\rho} = 9 \quad (3.26)$$

introduces additional uncertainty – up to an order of magnitude in the cross section and a factor of a few in the mass, for example. However, Ref. [54] have chosen to understate their bound by a factor of about 4, and so numerically the bound does not change by more than a factor of 2.

However, the bound is in fact even more subtle. The above calculation takes into account multiple scattering of an individual dark matter particle with multiple halo particles. But it neglects the interactions of the dark matter particles inside the dwarf – where dark matter is far denser and slower – leading to core formation and potential core collapse, as discussed in section 4.1 below. Allowing for this effect redistributes energy so that rather than eventually lifting a particle to escape velocity, the multiple scatterings of all dark matter particles can redistribute dark matter in the dwarf galaxy itself. How this does so requires a full detailed calculation. But it seems likely that dwarfs will puff out so that smaller dwarfs will become bigger in size – and also slow down core collapse to make them less dense in their cores. This is clearly of interest to evaluate further. For the purposes of this paper, we note only that these considerations may weaken the bound on darkly-charged dark matter.

3.3 Merging Cluster Constraints

Merging galaxy clusters are unique probes of the large velocity limit of the dark matter self-interaction cross section [49–59]. Detailed observations of merging clusters lead to different types of dark matter constraints, including those based on the gas and dark matter offset, the high velocity of the subclusters after the initial collision, the survival of distinct dark matter-dominated mass peaks after the collision, and the possible presence of an offset between the mass peak and the galaxy centroid. For the Bullet cluster [49, 50], the two latter techniques yield the most stringent constraint. This result was used in Ref. [8] to impose an additional bound on darkly-charged dark matter, albeit a very weak one due to the large relative velocities of the colliding clusters. We include this constraint in figure 4. However, this much weaker bound is itself subject to mitigating factors. For instance, we know only the dark matter and baryonic densities after the merger and the initial conditions are entirely unknown. It is not even known whether the ratio of baryonic to dark matter components is the same for the two merging clusters. For this reason, we don’t know enough about the fraction of the initial dark matter component that can be removed through scattering. Recently, Ref. [59] has shown that uncertainties associated with the measurement technique used to extract the dark matter-galaxy offset can even supersede the above concerns, leading to a weakening of this already feeble bound.

As more merging clusters are analyzed [51–58] and systematics become better understood, they could eventually provide improved constraints on the dark matter self-interaction strength. Still, given the strong suppression at large velocities of the transfer cross section for darkly-charged dark matter, it is unlikely that merging clusters will ever provide the strongest bound on our model.

4 For the Future

We have presented an updated calculation of the rate at which one population of stars would transfer velocity to another, or for the case of interest the rate at which large components of velocity would transfer energy to other velocity components. We have shown that the constraint on the interaction cross section is weaker than previously claimed, allowing for lighter dark matter particle or a larger charge – assuming a massless photon in the dark sector. In this section, we present a number of open issues that would be essential to pinning down the strongest constraint on darkly charged dark matter and perhaps indicating a way forward in terms of the search for interactivity.

As explained, the ellipticity constraint as calculated might still be overly strong. We know that the connection between an isotropic distribution of velocities and an isotropic potential is robust only for isolated and relaxed halos. The constraint we presented was based on the assumption that the timescale for isotropizing velocities is similar to that necessary to remove any anisotropies in the gravitational potential itself. A dedicated cosmological simulation of a dark matter halo with Coulomb-like interactions would probe the interplay between velocity and potential isotropy, and assess whether our assumption is justified. A potentially interesting direction will be to see if radial dependence can help distinguish the two sources of anisotropy, at least on a statistical basis. Ellipticity changes with radius, and it would be less likely for strong changes to be associated with anisotropy in velocities.

Another extremely interesting area for study is the interaction of the dwarf galaxies with their host haloes. Dark matter self-interaction can inject heat into the dwarves, and can interplay with self-interaction within the dwarf (we consider the strong self-interaction within dwarves in more detail in section 4.1). This will lead to modifications of the mass function and internal structure of dwarf galaxies should there be significant interaction, affecting the predictions that should be compared with observations. For instance, we expect to find fewer dwarf galaxies than would otherwise predicted since some will evaporate. Furthermore we expect the density profile of dwarf satellite galaxies to evolve toward bigger, less dense objects with potential implications for core-cusp issues [62, 63, 65] and the Too Big to Fail problem [64]. Again, we leave this for further work.

The third type of constraint we discussed arises from merging cluster observations. Due to the large typical velocities of these merging systems, they yield weaker bounds on darkly-charged dark matter than the dwarf galaxy survival constraint. As outlined above, modeling uncertainties and possible systematics in the measurement techniques can further weaken the constraints, although we can expect those to come under better control as more clusters are analyzed. It is of interest to see what we can learn from these types of objects in the future as well, particularly if there are separate dark matter populations with various degrees of interactivity. As emphasized in Ref. [55], it might even be possible to distinguish dark matter models with a contact-type interaction from models displaying long-range forces such as darkly-charged dark matter, an intriguing possibility.

One of the most interesting aspects of darkly-charged dark matter, and one that is the hardest to quantify, is the possible presence of collective plasma effects within the dark sector. The massless dark photon allows for a range of phenomena such as plasma waves, magnetic instabilities, and shocks [78, 79] that all could be relevant to small-scale structures. For instance, Ref. [7] determined that the Weibel plasma instability could be relevant for the entire darkly-charged dark matter parameter space. Detailed magnetohydrodynamics simulations would be required to fully understand whether this can lead to new constraints on this darkly-charged dark matter.

As we have already mentioned, many of the arguments we present rely on assumptions about the unknown initial state of a given galaxy or clusters of galaxies. In the case of a galaxy, we have only one well measured system – NGC720. However, having a larger statistical sample of these objects would help make the constraints more robust and, to a certain extent, eliminate the initial state dependence. This is especially the case for elliptical galaxies. Measurement of the ellipticity of dwarf galaxies can potentially yield a stronger constraint since we expect our self-interaction cross section to be bigger in colder systems.

4.1 Cores in Very Strongly Interacting Systems

One final consideration applies only in the presence of interactions as strong as those we have shown to be permissible. Self-interacting systems can affect the structure of dark matter haloes at cluster, galaxy, and dwarf galaxy scales. In principle, self-interacting systems can lead to core formation by allowing heat to flow from the outer part of a galaxy to the center and thereby expanding a central, initially cuspy region. With stronger interactions still, core collapse can occur on galactic time scales [80, 81].

This type of gravothermal collapse arises in a number of astrophysical settings such as globular clusters, and during star and planet formation. The core collapse in dark matter haloes can be studied in analogy with these systems. The rate of collapse is determined by the rate of heat transfer from the center of the system to outside, which depends on the temperature and density of the system, which can be very different in different cases. In some cases nuclear forces provide an additional heat source.

For dark matter haloes the rate of heat loss can be offset by the presence of a host halo or from cosmological infall, which can provide an external source of heat input slowing down or stopping gravothermal collapse [69]. This can lead to a difference in halo properties for dwarves in host galaxies and isolated dwarves.

A critical quantity characterizing the thermal evolution of the system is the Knudsen number

$$Kn = \frac{\lambda}{R} \tag{4.1}$$

defined as the ratio of mean free path λ to the size of the object R . This tells us how effective scattering is within an object of a given size. For small cross sections and hence large Knudsen numbers, $Kn > 1$, the conductivity is inversely proportional to Kn . Specifically, $Kn \gg 1$ ($\sigma \rightarrow 0$) corresponds to essentially collisionless dark matter. For $Kn \gtrsim 1$, heat conduction is effective and leads to core formation on galactic timescales through transfer of heat from the outer parts of the halo to the inside. For even stronger cross sections, the direction of the heat flow can reverse [80] and the core can undergo a collapse exhibiting gravothermal catastrophe. But for $Kn \ll 1$, (small mean free path), heat conduction is suppressed, and hence both core formation and core collapse are inhibited. Therefore, for extremely strong interactions the system might more closely resemble the non-interacting one [68, 69].

This leads to the rather remarkable possibility that sufficiently strong interactions can lead to density profiles different from either a non-interacting system or the SIDM models that have already been studied. In our case, the cross section of interest is highly velocity dependent. In various systems, dwarf galaxies, galaxies and clusters, we calculate a cross section for self-interactions of order

$$\frac{\sigma_T}{m_X} = \frac{8\pi\alpha_D^2}{m_X^3 v^4} \log \Lambda = \begin{cases} 1.7 \times 10^4 \frac{\text{cm}^2}{\text{g}} \left(\frac{\alpha_D}{2.5 \times 10^{-3}}\right)^2 \left(\frac{100 \text{ GeV}}{m_X}\right)^3 \left(\frac{\log \Lambda}{45}\right) \left(\frac{30 \text{ km/s}}{v}\right)^4 & \text{Dwarf galaxies} \\ 2.1 \times 10^0 \frac{\text{cm}^2}{\text{g}} \left(\frac{\alpha_D}{2.5 \times 10^{-3}}\right)^2 \left(\frac{100 \text{ GeV}}{m_X}\right)^3 \left(\frac{\log \Lambda}{60}\right) \left(\frac{300 \text{ km/s}}{v}\right)^4 & \text{Galaxies} \\ 2.0 \times 10^{-2} \frac{\text{cm}^2}{\text{g}} \left(\frac{\alpha_D}{2.5 \times 10^{-3}}\right)^2 \left(\frac{100 \text{ GeV}}{m_X}\right)^3 \left(\frac{\log \Lambda}{72}\right) \left(\frac{1000 \text{ km/s}}{v}\right)^4 & \text{Clusters.} \end{cases} \quad (4.2)$$

The interaction cross section in dwarf galaxies is several orders of magnitude greater than the value for which Ref. [40] found evidence for core collapse. For these values of the parameters, we can estimate the Knudsen numbers in various systems,

$$Kn \simeq \begin{cases} 10^{-3} \left(\frac{1 \text{ kpc}}{R}\right) \left(\frac{9 \text{ GeV/cm}^3}{\rho}\right) \left(\frac{1.7 \times 10^4 \text{ cm}^2/\text{g}}{\sigma_T/m_X}\right) & \text{Dwarf galaxies} \\ 10^1 \left(\frac{30 \text{ kpc}}{R}\right) \left(\frac{0.3 \text{ GeV/cm}^3}{\rho}\right) \left(\frac{2.1 \text{ cm}^2/\text{g}}{\sigma_T/m_X}\right) & \text{Galaxies} \\ 10^5 \left(\frac{10 \text{ Mpc}}{R}\right) \left(\frac{9 \times 10^{-6} \text{ GeV/cm}^3}{\rho}\right) \left(\frac{2.0 \times 10^{-2} \text{ cm}^2/\text{g}}{\sigma_T/m_X}\right) & \text{Clusters.} \end{cases} \quad (4.3)$$

We see that for dark matter as light and as strongly interacting as we have found is allowed, we can be in the very small Kn regime for dwarf galaxies, with a transition to the more standard SIDM scenario as velocity increases and density decreases. It is worth noting that if the constraints on α_D were an order of magnitude stronger, the smallest Knudsen numbers in the dwarf galaxies would be $\mathcal{O}(1)$. Therefore, the weaker bounds in α_D that we have found open up the small Knudsen number region in dwarf galaxies. It is unclear without a more detailed analysis what the consequences will be, leaving open the interesting possibility that this velocity-dependent cross section can evade other bounds but have interesting consequences in dwarf galaxies.

One way to interpret this result is in terms of a “cut-off” beyond which the system goes over to an effective more weakly interacting theory, presumably by coarse-graining over the mean-free path. Because a cutoff is automatically imposed by the strong interactions that occur at small velocity, this opens the possibility of fitting to observed galaxy and galaxy cluster shapes over a wide range of scales. Ref. [46] worked with available data to fit cores to different-sized objects, ranging from galaxy clusters to dwarf galaxies. Our cross section for clusters ($0.02 \text{ cm}^2/\text{g}$) is somewhat smaller than their best fit ($\sim 0.1 \text{ cm}^2/\text{g}$), but may be consistent with core formation in clusters. The cross section at galaxy scales is on the larger side ($1\text{--}10 \text{ cm}^2/\text{g}$), but again may be consistent within uncertainties. However, our cross section at the low velocity scales in dwarf galaxies is huge ($10^4 \text{ cm}^2/\text{g}$), since it scales as $1/v^4$. In order to fit to a much lower cross section ($1 \text{ cm}^2/\text{g}$), Ref. [46] imposed a mass for the mediator to cut off the cross section at low velocities. It is interesting to note that there may be no need for such a mass for the mediator since the short-mean-free path serves as a dynamic cutoff at small velocity. In fact, refs. [68, 69] seems to indicate an approximate duality $Kn \rightarrow 1/Kn$ between the strongly and weakly interacting regimes. It will be interesting to explore the robustness of this rough symmetry. Furthermore, the

authors of Ref. [68] indicated that the value of $10^4 \text{ cm}^2/\text{g}$ that are relevant for the dwarf galaxies in our model (see eq. (4.2) above) might lead to core formation similar to that of standard SIDM.

Here, we have explored just a few target systems and velocities. In reality, there is a broad range of objects with velocity dispersions spanning the values between those of the large galaxies and dwarf galaxies that we listed in eq. (4.2). In principle, our model makes a strong prediction for the properties of these intermediate objects since the cross section increases dramatically as we go from large galaxies to the smallest dwarves. Over a significant range, the dark matter interaction strength will be sufficiently weak that we expect results can be found reliably at this point and compared to data. The strong velocity dependence of a cross-section provided by a massless mediator should allow for the most stringent tests of this model, and perhaps ways to even discover the massless dark photon processes in the future.

Clearly the photon-mediated velocity-dependent cross section provides an extremely rich interesting system. It is remarkable that the necessary cutoff appears to be automatically imposed by the strong interactions that occur at small velocity. In a future analysis we envision imposing an effective theory, in which strongly interacting regimes would be replaced by more weakly interacting ones by coarse-graining over mean free paths. This should provide an approximate realization of this system and might even allow for a fit to cores over a wide range of scales.

For now, we note that the core constraint is an important one. It nonetheless does not currently rule out the interesting darkly-charged dark matter scenario that we envision.

5 Conclusions

We have argued that darkly-charged dark matter, where dark matter experiences a long range force not experienced by ordinary Standard Model matter, is a viable possibility with extremely rich phenomenology. We have shown that the allowed parameter space is considerably less restrictive than previously assumed and dark matter can be as light as the weak scale, 100 GeV, and still experience significant interactions: $\alpha_D = 2.5 \times 10^{-3}$, where even this constraint, which comes from relic abundance, can change in more elaborate models. The renewed parameter space is important as it says that dark matter, which we take to be relatively inert, can conceivably have reasonably strong interactions and have mass comparable to that of known Standard Model particles and still be consistent with known observations. Intriguingly, the weaker bounds also open up parameter space for novel dark matter halo dynamics such that dark matter in dwarf galaxies can be strongly self-interacting. Such interactions inhibit heat flow over scales larger than the mean free path, introducing a dynamical cutoff to the self-interactions.

In a companion paper [61], we consider the case where in addition to the weak-scale X dark matter particle, there is a light dissipative component which can lead to a dark matter disk. Unlike the previous study [34, 35] where the halo comprised of a separate CDM species, all of dark matter would be composed of charged components. This has additional interesting consequences for the formation of structure in the early universe.

Although current constraints are relatively weak, they lie at the boundary of the favored region where darkly-charged dark matter can be a thermal relic. Consequently, future observations may be able probe this extremely promising region and provide the opportunity to learn more about the nature of dark matter. In particular, charged dark matter can affect

the distribution of structure in the Universe and might ultimately provide a better match to data. Given our lack of knowledge about the nature of dark matter, darkly-charged dark matter is a simple possibility worth considering which we might have experimental access to in the near future.

Acknowledgments

We thank Sasha Brownsberger, Doug Finkbeiner, Gil Holder, Annika Peter, Subir Sarkar, Neal Weiner, Linda Xu, Hai-Bo Yu, and Kathryn Zurek for useful discussions. We thank Manoj Kaplinghat for useful comments on an earlier version of this manuscript. F.-Y. C.-R. acknowledges the support of the National Aeronautical and Space Administration ATP grant NNX16AI12G at Harvard University. This work is supported by NSF grants PHY-0855591 and PHY-1216270. We would like to thank the Aspen Center for Physics, the Mainz Institute for Theoretical Physics, and David Rubenstein for hospitality during the completion of this work.

A Scattering Cross-section

The process for $XX \rightarrow XX$ and $\bar{X}\bar{X} \rightarrow \bar{X}\bar{X}$ corresponds to Møller scattering. The process responsible for $X\bar{X} \rightarrow X\bar{X}$ represents Bhabha scattering. The cross section, in the CM frame, for Møller process is:

$$\frac{d\sigma}{d\Omega} = \frac{\alpha_D^2}{2s} \left(\frac{s^2 + u^2 + 8m^2t - 8m^4}{t^2} + \frac{s^2 + t^2 + 8m^2u - 8m^4}{u^2} + \frac{2s^2 - 16m^2s + 24m^4}{ut} \right). \quad (\text{A.1})$$

where s, t, u are the usual Mandelstam variables. They can be parametrized as,

$$s = 4m^2 + 4m^2v_{\text{cm}}^2 + \mathcal{O}(v_{\text{cm}}^4) \quad (\text{A.2})$$

$$t = -\frac{1}{2}(s - 4m^2)(1 - \cos\theta_{\text{cm}}) \quad (\text{A.3})$$

$$u = -\frac{1}{2}(s - 4m^2)(1 + \cos\theta_{\text{cm}}) \quad (\text{A.4})$$

The Bhabha scattering cross-section can be obtained by $s \leftrightarrow u$ crossing symmetry. To the lowest order in v_{cm} we recover the differential cross section for Møller process:

$$\frac{d\sigma_{\text{cm}}}{d\Omega} = \frac{\alpha_D^2}{4m^2v_{\text{cm}}^4(1 - \cos\theta_{\text{cm}})^2} \frac{(1 + 3\cos^2\theta_{\text{cm}})}{(1 + \cos\theta_{\text{cm}})^2} \quad (\text{A.5})$$

Notice that this cross-section diverges for both $\theta_{\text{cm}} = 0$ and π . However, because of the indistinguishable final state particles, we only consider the range $0 < \theta_{\text{cm}} < \pi/2$. Similarly the lowest order in v_{cm} the Bhabha process gives:

$$\frac{d\sigma_{\text{cm}}}{d\Omega} = \frac{\alpha_D^2}{4m^2v_{\text{cm}}^4(1 - \cos\theta_{\text{cm}})^2} \quad (\text{A.6})$$

This process has only singularity for $\theta = 0$ and the full range $0 < \theta_{\text{cm}} < \pi$, because X and \bar{X} are distinguishable. Since our cross-sections will be dominated by their singular behavior

at $\theta_{\text{cm}} = 0$, we only need to use the θ_{cm}^{-4} terms for which the Møller and Bhabha processes agree:

$$\frac{d\sigma_{\text{cm}}}{d\Omega} \sim \frac{4\alpha_D^2}{m^2|v_1 - v_2|^4(1 - \cos\theta_{\text{cm}})^2} = \frac{\alpha_D^2}{16m^2v_{\text{cm}}^4 \sin^4 \frac{\theta_{\text{cm}}}{2}} \quad (\text{A.7})$$

As a side note, we remark that this cross section agrees with that used in Ref. [54] in the $\theta \rightarrow 0$ limit.

We note that the cross sections above are obtained in the Born approximation; a more appropriate regime for our calculation would be the classical regime [19, 20], where multi-photon processes also contribute. For the massless mediator, however, the Born and classical differential cross sections are the same, and the difference only appears in the IR cutoff used to calculate the momentum transfer cross section. For a massive mediator, the mass provides an automatic IR cutoff so that the classical and Born calculations differ [19, 20]. Our computations in the text agree with the classical cross sections in Ref. [82] (except we use the inter-particle spacing as the screening length).

B Differential equation for velocity anisotropy

The goal of this Appendix is to simplify the expression:

$$-\frac{3\dot{v}_c}{v_c^4} = \frac{32\pi^3\sqrt{\pi}\alpha_D^2}{m^2n_c} \int \frac{dv_2}{v_2} \frac{dx}{(1-x)^2} \left[f(0)f(v_2) - f(v_2\sqrt{(1-x)/2})f(v_2\sqrt{(1+x)/2}) \right] \quad (\text{B.1})$$

Let us first consider the term in the brackets:

$$\begin{aligned} G &= f(0)f(v_2) - f(v_2\sqrt{(1-x)/2})f(v_2\sqrt{(1+x)/2}) \\ &= \left[\frac{n_c}{v_c^3} + \frac{n_h}{v_h^3} \right] \left[\frac{n_c}{v_c^3} e^{-\frac{v_2^2}{v_c^2}} + \frac{n_h}{v_h^3} e^{-\frac{v_2^2}{v_h^2}} \right] - \left[\frac{n_c}{v_c^3} e^{-\frac{v_2^2(1-x)}{2v_c^2}} + \frac{n_h}{v_h^3} e^{-\frac{v_2^2(1-x)}{2v_h^2}} \right] \left[\frac{n_c}{v_c^3} e^{-\frac{v_2^2(1+x)}{2v_c^2}} + \frac{n_h}{v_h^3} e^{-\frac{v_2^2(1+x)}{2v_h^2}} \right] \end{aligned}$$

All the terms proportional to n_c^2 and n_h^2 cancel because each Gaussian is already an equilibrium distribution. Therefore only cross-terms are left:

$$G = \frac{n_h n_c}{v_h^3 v_c^3} \left(e^{-\frac{v_2^2}{v_c^2}} + e^{-\frac{v_2^2}{v_h^2}} - e^{-\frac{v_2^2(1+x)}{2v_c^2}} e^{-\frac{v_2^2(1-x)}{2v_h^2}} - e^{-\frac{v_2^2(1-x)}{2v_c^2}} e^{-\frac{v_2^2(1+x)}{2v_h^2}} \right) \quad (\text{B.2})$$

Since we are interested in the $\theta' \rightarrow 0$, i.e. $x \rightarrow 1$ limit, we expand G around $x = 1$:

$$G = n_h n_c \frac{v_2^2 (v_c^2 - v_h^2)}{2 v_c^5 v_h^5} \left(e^{-v_2^2/v_c^2} - e^{-v_2^2/v_h^2} \right) (1-x) + \mathcal{O}[(1-x)^2]. \quad (\text{B.3})$$

Combining equations (B.1) and (B.3) we obtain

$$\dot{v}_c = -\frac{16\pi^3\sqrt{\pi}\alpha_D^2 n_h (v_c^2 - v_h^2)}{3m^2 v_c v_h^5} \int v_2 dv_2 \left(e^{-v_2^2/v_c^2} - e^{-v_2^2/v_h^2} \right) \int \frac{dx}{(1-x)} \quad (\text{B.4})$$

Finally, the integral over v_2 is simple and we obtain a simple expression for \dot{v}_c :

$$\dot{v}_c = -\frac{8\pi^3\sqrt{\pi}\alpha_D^2 n_h (v_c^2 - v_h^2)^2}{3m^2 v_c v_h^5} \int_0^{\cos^{-1}\theta_{\text{min}}} \frac{dx}{(1-x)} \quad (\text{B.5})$$

References

- [1] H. Goldberg and L. J. Hall, *A New Candidate for Dark Matter*, *Phys. Lett.* **B174** (1986) 151.
- [2] B. Holdom, *Searching for charges and a new $u(1)$* , *Physics Letters B* **178** (1986) 65 – 70.
- [3] B.-A. Gradwohl and J. A. Frieman, *Dark matter, long-range forces, and large-scale structure*, *Astrophys. J.* **398** (Oct., 1992) 407–424.
- [4] E. D. Carlson, M. E. Machacek and L. J. Hall, *Self-interacting dark matter*, *Astrophys. J.* **398** (Oct., 1992) 43–52.
- [5] R. Foot, *Mirror matter-type dark matter*, *Int. J. Mod. Phys.* **D13** (2004) 2161–2192, [[astro-ph/0407623](#)].
- [6] J. L. Feng, H. Tu and H.-B. Yu, *Thermal Relics in Hidden Sectors*, *JCAP* **0810** (2008) 043, [[0808.2318](#)].
- [7] L. Ackerman, M. R. Buckley, S. M. Carroll and M. Kamionkowski, *Dark Matter and Dark Radiation*, *Phys. Rev. D* **79** (2009) 023519, [[0810.5126](#)].
- [8] J. L. Feng, M. Kaplinghat, H. Tu and H.-B. Yu, *Hidden Charged Dark Matter*, *JCAP* **0907** (2009) 004, [[0905.3039](#)].
- [9] J. L. Feng, M. Kaplinghat and H.-B. Yu, *Halo Shape and Relic Density Exclusions of Sommerfeld-Enhanced Dark Matter Explanations of Cosmic Ray Excesses*, *Phys. Rev. Lett.* **104** (2010) 151301, [[0911.0422](#)].
- [10] N. Arkani-Hamed, D. P. Finkbeiner, T. R. Slatyer and N. Weiner, *A Theory of Dark Matter*, *Phys. Rev. D* **79** (2009) 015014, [[0810.0713](#)].
- [11] D. E. Kaplan, G. Z. Krnjaic, K. R. Rehermann and C. M. Wells, *Atomic Dark Matter*, *Journal of Cosmology and Astroparticle Physics* **1005** (2010) 021, [[0909.0753](#)].
- [12] M. R. Buckley and P. J. Fox, *Dark matter self-interactions and light force carriers*, *Phys. Rev. D* **81** (Apr., 2010) 083522, [[0911.3898](#)].
- [13] D. E. Kaplan, G. Z. Krnjaic, K. R. Rehermann and C. M. Wells, *Dark Atoms: Asymmetry and Direct Detection*, *Journal of Cosmology and Astroparticle Physics* **1110** (2011) 011, [[1105.2073](#)].
- [14] S. R. Behbahani, M. Jankowiak, T. Rube and J. G. Wacker, *Nearly Supersymmetric Dark Atoms*, *Adv. High Energy Phys.* **2011** (2011) 709492, [[1009.3523](#)].
- [15] S. Das and K. Sigurdson, *Cosmological limits on hidden sector dark matter*, *Phys. Rev. D* **85** (2012) 063510, [[1012.4458](#)].
- [16] D. Hooper, N. Weiner and W. Xue, *Dark Forces and Light Dark Matter*, *Phys. Rev. D* **86** (2012) 056009, [[1206.2929](#)].
- [17] L. G. van den Aarssen, T. Bringmann and C. Pfrommer, *Is dark matter with long-range interactions a solution to all small-scale problems of Λ CDM cosmology?*, *Phys. Rev. Lett.* **109** (2012) 231301, [[1205.5809](#)].
- [18] J. M. Cline, Z. Liu and W. Xue, *Millicharged Atomic Dark Matter*, *Phys. Rev. D* **85** (2012) 101302, [[1201.4858](#)].
- [19] S. Tulin, H.-B. Yu and K. M. Zurek, *Beyond Collisionless Dark Matter: Particle Physics Dynamics for Dark Matter Halo Structure*, *Phys. Rev. D* **87** (2013) 115007, [[1302.3898](#)].
- [20] S. Tulin, H.-B. Yu and K. M. Zurek, *Resonant Dark Forces and Small Scale Structure*, *Phys. Rev. Lett.* **110** (2013) 111301, [[1210.0900](#)].
- [21] M. Baldi, *Structure formation in Multiple Dark Matter cosmologies with long-range scalar interactions*, *Mon. Not. R. Astron. Soc.* **428** (2013) 2074, [[1206.2348](#)].

- [22] F.-Y. Cyr-Racine and K. Sigurdson, *The cosmology of atomic dark matter*, *Phys. Rev. D* **87** (2013) 103515, [[1209.5752](#)].
- [23] J. M. Cline, Z. Liu, G. Moore and W. Xue, *Composite strongly interacting dark matter*, *Phys. Rev. D* **90** (2014) 015023, [[1312.3325](#)].
- [24] X. Chu and B. Dasgupta, *Dark Radiation Alleviates Problems with Dark Matter Halos*, *Phys. Rev. Lett.* **113** (2014) 161301, [[1404.6127](#)].
- [25] J. M. Cline, Z. Liu, G. Moore and W. Xue, *Scattering properties of dark atoms and molecules*, *Phys. Rev. D* **89** (2014) 043514, [[1311.6468](#)].
- [26] T. Bringmann, J. Hasenkamp and J. Kersten, *Tight bonds between sterile neutrinos and dark matter*, *JCAP* **1407** (2014) 042, [[1312.4947](#)].
- [27] E. Gabrielli and M. Raidal, *Exponentially spread dynamical Yukawa couplings from nonperturbative chiral symmetry breaking in the dark sector*, *Phys. Rev.* **D89** (2014) 015008, [[1310.1090](#)].
- [28] K. K. Boddy, J. L. Feng, M. Kaplinghat and T. M. P. Tait, *Self-Interacting Dark Matter from a Non-Abelian Hidden Sector*, *Phys. Rev. D* **89** (2014) 115017, [[1402.3629](#)].
- [29] M. Archidiacono, S. Hannestad, R. S. Hansen and T. Tram, *Cosmology with self-interacting sterile neutrinos and dark matter - A pseudoscalar model*, *Phys. Rev. D* **91** (2015) 065021, [[1404.5915](#)].
- [30] J. Choquette and J. M. Cline, *Minimal nonabelian model of atomic dark matter*, [1509.05764](#).
- [31] M. A. Buen-Abad, G. Marques-Tavares and M. Schmaltz, *Non-Abelian dark matter and dark radiation*, *Phys. Rev.* **D92** (2015) 023531, [[1505.03542](#)].
- [32] P. Ko and Y. Tang, *Residual Non-Abelian Dark Matter and Dark Radiation*, [1609.02307](#).
- [33] T. Bringmann, H. T. Ihle, J. Kersten and P. Walia, *Suppressing structure formation at dwarf galaxy scales and below: late kinetic decoupling as a compelling alternative to warm dark matter*, [1603.04884](#).
- [34] J. J. Fan, A. Katz, L. Randall and M. Reece, *Dark-Disk Universe*, *Phys. Rev. Lett.* **110** (2013) 211302, [[1303.3271](#)].
- [35] J. Fan, A. Katz, L. Randall and M. Reece, *Double-Disk Dark Matter*, *Phys. Dark Univ.* **2** (2013) 139–156, [[1303.1521](#)].
- [36] F.-Y. Cyr-Racine, R. de Putter, A. Raccanelli and K. Sigurdson, *Constraints on Large-Scale Dark Acoustic Oscillations from Cosmology*, *Phys. Rev.* **D89** (2014) 063517, [[1310.3278](#)].
- [37] Z. Chacko, Y. Cui, S. Hong, T. Okui and Y. Tsai, *Partially Acoustic Dark Matter, Interacting Dark Radiation, and Large Scale Structure*, [1609.03569](#).
- [38] M. Kesden and M. Kamionkowski, *Tidal Tails Test the Equivalence Principle in the Dark Sector*, *Phys. Rev.* **D74** (2006) 083007, [[astro-ph/0608095](#)].
- [39] A. Schneider, *Astrophysical constraints on resonantly produced sterile neutrino dark matter*, *JCAP* **1604** (2016) 059, [[1601.07553](#)].
- [40] M. Vogelsberger, J. Zavala and A. Loeb, *Subhaloes in Self-Interacting Galactic Dark Matter Haloes*, *Mon. Not. R. Astron. Soc.* **423** (2012) 3740, [[1201.5892](#)].
- [41] J. Zavala, M. Vogelsberger and M. G. Walker, *Constraining Self-Interacting Dark Matter with the Milky Way’s dwarf spheroidals*, *Mon. Not. R. Astron. Soc.* **431** (2013) L20–L24, [[1211.6426](#)].
- [42] M. Vogelsberger and J. Zavala, *Direct detection of self-interacting dark matter*, *Mon. Not. R. Astron. Soc.* **430** (2013) 1722–1735, [[1211.1377](#)].

- [43] M. Vogelsberger, J. Zavala, C. Simpson and A. Jenkins, *Dwarf galaxies in CDM and SIDM with baryons: observational probes of the nature of dark matter*, *Mon. Not. R. Astron. Soc.* **444** (2014) 3684, [[1405.5216](#)].
- [44] C. Boehm, J. A. Schewtschenko, R. J. Wilkinson, C. M. Baugh and S. Pascoli, *Using the Milky Way satellites to study interactions between cold dark matter and radiation*, *Mon. Not. Roy. Astron. Soc.* **445** (2014) L31–L35, [[1404.7012](#)].
- [45] M. R. Buckley, J. Zavala, F.-Y. Cyr-Racine, K. Sigurdson and M. Vogelsberger, *Scattering, Damping, and Acoustic Oscillations: Simulating the Structure of Dark Matter Halos with Relativistic Force Carriers*, *Phys. Rev. D* **90** (2014) 043524, [[1405.2075](#)].
- [46] M. Kaplinghat, S. Tulin and H.-B. Yu, *Dark Matter Halos as Particle Colliders: Unified Solution to Small-Scale Structure Puzzles from Dwarfs to Clusters*, *Phys. Rev. Lett.* **116** (2016) 041302, [[1508.03339](#)].
- [47] J. A. Schewtschenko, R. J. Wilkinson, C. M. Baugh, C. Boehm and S. Pascoli, *Dark matter-radiation interactions: the impact on dark matter haloes*, *Mon. Not. R. Astron. Soc.* **449** (2015) 3587–3596, [[1412.4905](#)].
- [48] M. Vogelsberger, J. Zavala, F.-Y. Cyr-Racine, C. Pfrommer, T. Bringmann and K. Sigurdson, *ETHOS - an effective theory of structure formation: dark matter physics as a possible explanation of the small-scale CDM problems*, *Mon. Not. R. Astron. Soc.* **460** (Aug., 2016) 1399–1416, [[1512.05349](#)].
- [49] M. Markevitch, A. H. Gonzalez, D. Clowe, A. Vikhlinin, L. David, W. Forman et al., *Direct constraints on the dark matter self-interaction cross-section from the merging galaxy cluster 1E0657-56*, *Astrophys. J.* **606** (2004) 819–824, [[astro-ph/0309303](#)].
- [50] S. W. Randall, M. Markevitch, D. Clowe, A. H. Gonzalez and M. Bradac, *Constraints on the Self-Interaction Cross-Section of Dark Matter from Numerical Simulations of the Merging Galaxy Cluster 1E 0657-56*, *Astrophys. J.* **679** (2008) 1173–1180, [[0704.0261](#)].
- [51] W. A. Dawson, *The Dynamics of Merging Clusters: A Monte Carlo Solution Applied to the Bullet and Musket Ball Clusters*, *Astrophys. J.* **772** (2013) 131, [[1210.0014](#)].
- [52] I. Mohammed, J. Liesenborgs, P. Saha and L. L. R. Williams, *Mass-galaxy offsets in Abell 3827, 2218 and 1689: intrinsic properties or line-of-sight substructures?*, *Mon. Not. Roy. Astron. Soc.* **439** (2014) 2651–2661, [[1402.4217](#)].
- [53] W. A. Dawson, M. J. Jee, A. Stroe, Y. K. Ng, N. Golovich, D. Wittman et al., *MC²: Galaxy Imaging and Redshift Analysis of the Merging Cluster Ciza J2242.8+5301*, *Astrophys. J.* **805** (2015) 143, [[1410.2893](#)].
- [54] F. Kahlhoefer, K. Schmidt-Hoberg, M. T. Frandsen and S. Sarkar, *Colliding clusters and dark matter self-interactions*, *Mon. Not. Roy. Astron. Soc.* **437** (2014) 2865–2881, [[1308.3419](#)].
- [55] F. Kahlhoefer, K. Schmidt-Hoberg, J. Kummer and S. Sarkar, *On the interpretation of dark matter self-interactions in Abell 3827*, *Mon. Not. Roy. Astron. Soc.* **452** (2015) L54–L58, [[1504.06576](#)].
- [56] D. Harvey, R. Massey, T. Kitching, A. Taylor and E. Tittley, *The non-gravitational interactions of dark matter in colliding galaxy clusters*, *Science* **347** (2015) 1462–1465, [[1503.07675](#)].
- [57] R. Massey et al., *The behaviour of dark matter associated with four bright cluster galaxies in the 10 kpc core of Abell 3827*, *Mon. Not. Roy. Astron. Soc.* **449** (2015) 3393–3406, [[1504.03388](#)].
- [58] S. W. Randall, T. E. Clarke, R. J. van Weeren, H. T. Intema, W. A. Dawson, T. Mroczkowski et al., *Multi-wavelength Observations of the Dissociative Merger in the Galaxy Cluster CIZA J0107.7+5408*, *Astrophys. J.* **823** (2016) 94, [[1604.03551](#)].
- [59] A. Robertson, R. Massey and V. Eke, *What does the Bullet Cluster tell us about Self-Interacting Dark Matter?*, [1605.04307](#).

- [60] G. A. Dooley, A. H. G. Peter, M. Vogelsberger, J. Zavala and A. Frebel, *Enhanced tidal stripping of satellites in the galactic halo from dark matter self-interactions*, *Mon. Not. R. Astron. Soc.* **461** (Sept., 2016) 710–727, [[1603.08919](#)].
- [61] P. Agrawal, F.-Y. Cyr-Racine, L. Randall and J. Scholtz, *Dark Catalysis*, [1702.05482](#).
- [62] W. J. G. de Blok, *The Core-Cusp Problem*, *Advances in Astronomy* **2010** (2010) 789293, [[0910.3538](#)].
- [63] G. Gentile, P. Salucci, U. Klein, D. Vergani and P. Kalberla, *The Cored distribution of dark matter in spiral galaxies*, *Mon. Not. Roy. Astron. Soc.* **351** (2004) 903, [[astro-ph/0403154](#)].
- [64] M. Boylan-Kolchin, J. S. Bullock and M. Kaplinghat, *Too big to fail? The puzzling darkness of massive Milky Way subhaloes*, *Mon. Not. Roy. Astron. Soc.* **415** (2011) L40, [[1103.0007](#)].
- [65] M. G. Walker and J. Penarrubia, *A Method for Measuring (Slopes of) the Mass Profiles of Dwarf Spheroidal Galaxies*, *Astrophys. J.* **742** (2011) 20, [[1108.2404](#)].
- [66] O. Y. Gnedin and J. P. Ostriker, *Limits on collisional dark matter from elliptical galaxies in clusters*, *Astrophys. J.* **561** (2001) 61, [[astro-ph/0010436](#)].
- [67] B. Moore, S. Gelato, A. Jenkins, F. R. Pearce and V. Quilis, *Collisional versus collisionless dark matter*, *Astrophys. J.* **535** (2000) L21–L24, [[astro-ph/0002308](#)].
- [68] K. Ahn and P. R. Shapiro, *Formation and Evolution of Self-Interacting Dark Matter Halos*, *Journal of Korean Astronomical Society* **36** (Sept., 2003) 89–95, [[astro-ph/0212575](#)].
- [69] K.-J. Ahn and P. R. Shapiro, *Formation and evolution of the self-interacting dark matter halos*, *Mon. Not. Roy. Astron. Soc.* **363** (2005) 1092–1124, [[astro-ph/0412169](#)].
- [70] PLANCK collaboration, P. A. R. Ade et al., *Planck 2015 results. XIII. Cosmological parameters*, *Astron. Astrophys.* **594** (2016) A13, [[1502.01589](#)].
- [71] P. Gondolo and G. Gelmini, *Cosmic abundances of stable particles: Improved analysis*, *Nucl. Phys.* **B360** (1991) 145–179.
- [72] B. von Harling and K. Petraki, *Bound-state formation for thermal relic dark matter and unitarity*, *JCAP* **1412** (2014) 033, [[1407.7874](#)].
- [73] D. A. Buote, T. E. Jeltema, C. R. Canizares and G. P. Garmire, *Chandra evidence for a flattened, triaxial dark matter halo in the elliptical galaxy ngc 720*, *Astrophys. J.* **577** (2002) 183–196, [[astro-ph/0205469](#)].
- [74] P. J. Humphrey, D. A. Buote, C. R. Canizares, A. C. Fabian and J. M. Miller, *A Census of Baryons and Dark Matter in an Isolated, Milky Way Sized Elliptical Galaxy*, *Astrophys. J.* **729** (Mar., 2011) 53, [[1010.6078](#)].
- [75] A. H. G. Peter, M. Rocha, J. S. Bullock and M. Kaplinghat, *Cosmological Simulations with Self-Interacting Dark Matter II: Halo Shapes vs. Observations*, *Mon. Not. Roy. Astron. Soc.* **430** (2013) 105, [[1208.3026](#)].
- [76] M. Kaplinghat, R. E. Keeley, T. Linden and H.-B. Yu, *Tying Dark Matter to Baryons with Self-interactions*, *Phys. Rev. Lett.* **113** (2014) 021302, [[1311.6524](#)].
- [77] D. A. Buote and C. R. Canizares, *Geometrical evidence for dark matter: X-ray constraints on the mass of the elliptical galaxy NGC-720*, *Astrophys. J.* **427** (1994) 86, [[astro-ph/9311073](#)].
- [78] M. Heikinheimo, M. Raidal, C. Spethmann and H. Veermäe, *Dark matter self-interactions via collisionless shocks in cluster mergers*, *Physics Letters B* **749** (Oct., 2015) 236–241, [[1504.04371](#)].
- [79] T. Sepp, B. Deshev, M. Heikinheimo, A. Hektor, M. Raidal, C. Spethmann et al., *Simulations of Galaxy Cluster Collisions with a Dark Plasma Component*, [1603.07324](#).

- [80] S. Balberg, S. L. Shapiro and S. Inagaki, *Selfinteracting dark matter halos and the gravothermal catastrophe*, *Astrophys. J.* **568** (2002) 475–487, [[astro-ph/0110561](#)].
- [81] J. Koda and P. R. Shapiro, *Gravothermal collapse of isolated self-interacting dark matter haloes: N-body simulation versus the fluid model*, *Mon. Not. Roy. Astron. Soc.* **415** (2011) 1125, [[1101.3097](#)].
- [82] S. A. Khrapak, A. V. Ivlev, G. E. Morfill and S. K. Zhdanov, *Scattering in the Attractive Yukawa Potential in the Limit of Strong Interaction*, *Phys. Rev. Lett.* **90** (2003) 225002.